Salamander retina phospholipids and their localization by MALDI imaging mass spectrometry at cellular size resolution[S]

Michael C. Roy,[1,*] Hiroki Nakanishi,[2,†] Kazuteru Takahashi,[§] Setsuko Nakanishi,[*] Shigeki Kajihara,[§] Takahiro Hayasaka,[**] Mitsutoshi Setou,[**] Kiyoshi Ogawa,[§] Ryo Taguchi,[†] and Takayuki Naito[*]

Molecular Neuroscience Unit,* Okinawa Institute of Science and Technology (OIST), 12-22 Suzaki, Uruma, Okinawa 904-2234, Japan; Department of Metabolome, Graduate School of Medicine, The University of Tokyo, 7-3-1 Hongo, Bunkyo-ku, Tokyo 113-0033, Japan and Core Research for Evolutional Science and Technology,† 4-1-8 Honcho, Kawaguchi, Saitama 332-0012, Japan; Technology Research Laboratory, Shimadzu Corporation,§ 3-9-4 Soraku-gun, Seika-cho, Kyoto 619-0237, Japan; and Department of Molecular Anatomy,** Molecular Imaging Frontier Research Center, Hamamatsu University School of Medicine, 1-20-1 Handayama, Higashi-ku, Hamamatsu, Shizuoka 431-3192, Japan

Abstract Salamander large cells facilitated identification and localization of lipids by MALDI imaging mass spectrometry. Salamander retina lipid extract showed similarity with rodent retina lipid extract in phospholipid content and composition. Like rodent retina section, distinct layer distributions of phospholipids were observed in the salamander retina section. Phosphatidylcholines (PCs) composing saturated and monounsaturated fatty acids (PC 32:0, PC 32:1, and PC 34:1) were detected mainly in the outer and inner plexiform layers (OPL and IPL), whereas PCs containing polyunsaturated fatty acids (PC 36:4, PC 38:6, and PC 40:6) composed the inner segment (IS) and outer segment (OS). The presence of PCs containing polyunsaturated fatty acids in the OS layer implied that these phospholipids form flexible lipid bilayers, which facilitate phototransduction process occurring in the rhodopsin rich OS layer. Distinct distributions and relative signal intensities of phospholipids also indicated their relative abundance in a particular cell or a cell part. Using salamander large cells, a single cell level localization and identification of biomolecules could be achieved by MALDI imaging mass spectrometry.—Roy, M. C., H. Nakanishi, K. Takahashi, S. Nakanishi, S. Kajihara, T. Hayasaka, M. Setou, K. Ogawa, R. Taguchi, and T. Naito. **Salamander retina phospholipids and their localization by MALDI imaging mass spectrometry at cellular size resolution. *J. Lipid Res.* 2011.** 52: **463–470.**

Supplementary key words matrix-assisted laser desorption/ionization • *Ambystoma mexicanum* • lipidomics • phospholipid

Lipidomics has gained much attention in recent days due to lipids' crucial role in living systems. Lipids are chemically diverse biomolecules and their biological functions are also diverse in living cells. They are the principal components of cell membranes and control biomembrane physiology (1–3). The central nervous system is mostly composed of diverse lipids, and defective lipid metabolisms are related to various diseases of the brain and peripheral nervous systems (4). The retina, a part of the nervous system, receives light (photons) as information and transfers this information into electrophysiological signals to the brain. Photon-triggered electrochemical signal transduction occurs in the retina. The retina composes multilayers of neural cells, as shown in **Fig. 1**. A photochemical reaction occurs in the photoreceptor cells (rod and cone) outer segment (OS) harboring visual pigments. Rhodopsin (major visual pigment) function is highly correlated to the biomembranes' lipids composition. The rod's OS is mostly composed of lipids containing PUFAs, mainly docosahexaenoic acid (DHA; 22:6ω-3). DHA plays an important role in the development, survival, function, and in inhibiting apoptosis of retinal photoreceptors (5–8). PUFAs including DHA are in general susceptible to lipid

Manuscript received 15 August 2010 and in revised form 26 November 2010.

Published, JLR Papers in Press, December 13, 2010
DOI 10.1194/jlr.M010546

Abbreviations: AP, atmospheric pressure; CID, collision-induced dissociation; DHA, docosahexaenoic acid; GCL, ganglion cell layer; IMS, imaging mass spectrometry; INL, inner nuclear layer; IPL, inner plexiform layer; IS, inner segment; ITO, indium tin oxide; ONL, outer nuclear layer; OPL, outer plexiform layer; OS, outer segment; PC, phosphatidylcholine; RPE, retinal pigment epithelium.

[2] Present address of H. Nakanishi: Department of Biological Information Signal, Bioscience Education and Research Center, Akita University, Japan.

[1] To whom correspondence should be addressed.
e-mail:mcroy@oist.jp

[S] The online version of this article (available at http://www.jlr.org) contains supplementary data in the form of 14 figures and one table.

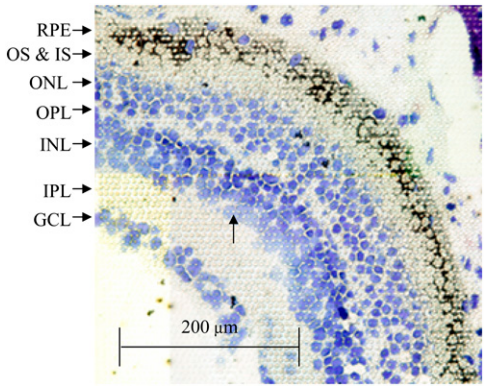

Fig. 1. An optical image of a salamander retina section visualized by toluidine blue staining after MALDI imaging mass data acquisition: RPE, retinal pigment epithelium; OS, outer segment; IS, inner segment; ONL, outer nuclear layer; OPL, outer plexiform layer; INL, inner nuclear layer; IPL, inner plexiform layer; GCL, ganglion cell layer. Small yellow dots represent laser spots (arrow). Frozen section, 5 μm, Bar: 200 μm.

peroxidation that is considered one of the causative factors of retinal diseases, such as age-related macular degeneration and diabetic retinopathy (9, 10). Because lipids are considered important causative and diagnostic molecules for retina diseases, a complete knowledge of the lipid profile of the normal retina is necessary (10).

Extraction of lipids from tissue followed by lipid characterization using HPLC MS and GC MS is the major direction in lipid research. However, spatial distribution of lipids in a given tissue is lost by the extraction method (1–3, 11, 12). To get information about spatial distribution of biomolecules in a given tissue, MALDI imaging mass spectrometry (IMS) is a versatile and robust method. IMS is gaining popularity for the analysis of biomolecules directly on tissue sections (13–17).

Using MALDI IMS, Hayasaka et al. (13) characterized four phosphatidylcholine (PC) molecules that were distributed in three distinct layers in a mouse retina section. The exclusive distribution of phospholipids containing DHA in the retinal OS and pigment epithelium has also been shown. Recently, their group also revealed fatty acid layer distribution in a mouse retina section using a nanoparticle-assisted laser desorption/ionization imaging mass spectrometry (nano-PALDI IMS) (14).

An experimental model animal, salamander (*Ambystoma mexicanum*), was selected to identify and visualize phospholipids in the retina section. Due to the salamander's large cells and a relatively simple nervous system, we envisage that it could be a suitable model animal for a single cell IMS study. As shown in Fig. 1, the salamander retina section has a similar basic structural organization with that of the mouse (13). Retinal pigment epithelium (RPE), OS and inner segment (IS), outer nuclear layer (ONL), outer plexiform layer (OPL), inner nuclear layer (INL), inner plexiform layer (IPL), and ganglion cell layer (GCL) are easily recognized. In addition, the salamander retinal cells (average diameter 14.5 μm) are larger than that of the mouse (average diameter 6.5 μm), and every layer contains fewer cells than the mouse retinal layer. The salamander retina having large cells and an atmospheric pressure (AP) MALDI IMS system having a more focused laser beam (<10 μm) enabled us to identify phospholipids at cellular size resolution. The narrow laser spots (small yellow dots, Fig. 1, arrow) are visible inside cells after toluidine blue staining. The AP MALDI MS instrument was equipped with a high resolution optical microscope that facilitated observation and selection of the target area of tissue samples for accurate analysis. ESI MS analyses of the salamander retina lipid extract also provided a complementary lipid profile.

MATERIALS AND METHODS

Chemicals and reagents

All solvents used were HPLC and LC-MS grade and other chemicals used were analytical grade (Wako Pure Chemicals, Japan). Ultrapure water was obtained from Milli-Q water system (Millipore, MA).

Preparation of retina section for MALDI IMS

A. mexicanum was anesthetized by 0.2% meta-aminobenzoic acid ethylester methanesulfonate (Sigma). Dissected eyeballs were rapidly frozen by liquid nitrogen-cooled isopentane. Five micron-thick frozen serial sections were cut on a cryostat (CM3050S, Leica, −20°C) and thaw mounted on an indium tin oxide (ITO) transparent (80%, λ = 550 nm) conductive film (100 Ω, Tobi Co. Ltd, Kyoto, Japan). The ITO film was pasted on the MALDI target plate using a double-sided conductive carbon tape. The carbon tape was pasted on the top of the ITO film. After MALDI IMS data acquisition, sections were stained by toluidine blue and photographed.

Matrix (2,5-dihydroxybenzoic acid, DHB) was coated on the retina sections by an evaporation method (18): evaporation condition, pressure <5 Pa; temperature, 130°C; time, 10 min; and amount of matrix, 30 mg. The matrix crystals were uniformly deposited on the tissue. The crystal size was about 1–2 μm (supplementary Fig. IX). The thickness error of matrix on the tissue was about 10% from center to edge but <1% in the analyzed area (analyzed area was about 1/100 of total tissue area.).

Preparation of retina lipid extract

Eyeballs were dissected from an anesthetized *A. mexicanum*. After dissection, retina was immediately separated from eyeballs and quickly frozen in liquid nitrogen. Isolated retina was kept at −80°C until lipid extraction. A pair of salamander retinas was homogenized with chloroform/methanol (1:2, v/v, 3 ml) using a glass homogenizer and total lipids were extracted using the Bligh-Dyer method (19). The total crude lipid extract was dried under a gentle nitrogen stream and redissolved in methanol (1 ml). The crude lipid sample was stored at −80°C until MS analysis.

LC-ESI MS analysis

ESI MS analysis was performed using a 4000 Q-TRAP® quadrupole-linear ion trap hybrid mass spectrometer (Applied Biosystems/MDS Sciex, Concord, ON, Canada) equipped with an Ultimate 3000 HPLC system (DIONEX Co., San Francisco, CA) or an ACQUITY Ultra Performance LC® (UPLC) (Waters, Millford, MA) combined with an HTC PAL autosampler (CTC Analytics, Zwingen, Switzerland). The conditions used for the 4000 Q-TRAP were as follows. The sample (5 μl) was subjected to ESI MS analysis by flow injection without LC separation. The mobile phase composition was acetonitrile/methanol/ammonium formate 50 mM (45:50:5, pH 7.4) at a flow rate 10 μl/min. The

scan range of the instrument was set at *m/z* 400–1200 at a scan speed of 1000 Da/s. The trap fill-time was set at 3 ms in the positive ion mode. Nitrogen was used as a curtain gas (setting of 10, arbitrary unit) and as a collision gas (set to high). The declustering potential was set at 20 V to minimize in-source fragmentation. Both Q1 and Q3 resolutions were set to unit mass. The collision energy used was varied according to the desired experiment. In order to identify the PC species, precursor ion and neutral loss scanning were performed; these methods are effective for the detection of phospholipids, because characteristic fragment ions or neutral losses are generated by collision-induced dissociation (CID).

LC-ESI MS analysis was carried out using an ACQUITY UPLC™ BEH C18 (150 mm × 1.0 mm, 1.7 μm) column. The crude lipid extract (10 μl) was injected into the column by an autosampler and separated by a step gradient using mobile phase A (acetonitrile/methanol/water 2:2:1, v/v/v, containing 0.1% formic acid and 0.028% ammonia) and mobile phase B (isopropanol containing 0.1% formic acid and 0.028% ammonia) at a flow rate 70 μl/min, and the column temperature was maintained at 30°C. The step gradient used was as follows: mobile phase A/mobile phase B 100:0 for 0–5 min, 95:5 for 5–20 min, 70:30 for 20–21 min, 50:50 for 21–84 min, and finally 100:0 for 84–100 min.

The MS/MS analysis was performed during LC-ESI MS measurement in negative ion mode. The ion spray voltage was set at −4500 V. Neutral loss scanning was performed to identify the PC species as described previously (20, 21). The characteristic fragmentation patterns of individual molecular PC species were determined by enhanced product ion scanning (EPI). These EPI experiments were performed as continuous data independent measurements for obtaining mass chromatograms of characteristic product ions. The collision energy was set at 45 eV. The scan range of the instrument was set at *m/z* 200–1000 at a scan speed of 1000 Da/s. The Q0 trapping was set to "ON". The linear ion trap fill-time was set at 10 ms. The declustering potential was set at −60 V. The resolution of Q1 was set to unit mass.

MALDI MS analysis

AP MALDI IMS data were acquired using a Mass Microscope (22). The Mass Microscope was developed by combining a LC-MS-IT-TOF (Shimadzu Corp., Kyoto, Japan) with a newly scanning AP MALDI system. The scanning AP MALDI system includes a high resolution optical microscope (40×) and a pulsed Nd:YAG laser (355 nm). The image resolution of the optical microscope is only a few micrometers. The laser irradiation area could be adjusted by defocusing the triplet lens, and the diffraction limit of the laser system is approximately 4 μm. These remarkable functions enabled us to detect the distribution of biomolecules on tissue sections at high spatial resolution. The following parameters were used for data collection: measurement mass range, *m/z* 550–1000; mass resolution, 10000; laser power, 0.11 μJ; laser shot pitch, 8 μm; laser spot size, ∼7 μm; number of pixels, 65 × 65 (Fig. 3) and 30 × 6 (Fig. 4) (positive ion mode); number of laser irradiations per pixel, 80.

MALDI IMS data processing

In-house built software and MATLAB™ version 7.5 (Mathworks, Inc.) were used for raw data saving, processing, and interpretation of IMS data. For principle component analysis (PCA), the hundred most intense peaks were picked from *m/z* 550–1000 at a mass tolerance of 0.5 Da. Pareto scaling was applied to reduce the relative importance of large peaks. PCA was carried out, and several principal components with high score were selected. VARIMAX rotation was applied to them in order to obtain more interpretable data.

Identification of PC species was based on their molecular mass ions (*m/z*), their various alkali metals adducts, and MS/MS analysis followed by a lipid database search (23). The imaging data and MS/MS data were obtained from the same retina section. When the product ions corresponded to specific neutral loss of trimethylamine, ($N(CH_3)_3$, 59 Da) and of cyclophosphane ring ($C_2H_5O_4P$, 124 Da) from a PC (supplementary Figs. X–XII) the *m/z* value of the PC precursor ion was searched against the lipid database. The data search provided total carbon number and unsaturated bond number included in the PC. Due to low population of precursor ions, we could not obtain detailed fatty acid composition of PC by MS/MS analysis. However, the corresponding PC with detailed fatty acid composition was unambiguously identified by MS/MS data obtained by LC-MS analysis of the crude lipid extract.

Using the AP MALDI MS system, we ran three experiments independently using at least three tissue sections from three animals and found the data to be reproducible (supplementary Fig. XIV).

RESULTS

Salamander retina phospholipids composition

Both positive and negative (supplementary Fig. I) ions ESI mass detected phospholipids in the salamander retina crude lipid extract. The most abundant phospholipids signals at *m/z* 732.6, 760.6, 782.6, 788.6, 806.6, 834.6, 878.5, and 906.6 were observed in the mass spectrum (**Table 1**), as shown in **Fig. 2**. Fatty acid composition in these lipid species varies from long-chain saturated fatty acids (FA 16:0) to very long-chain PUFAs (FA 36:6). A unique lipid (PC 44:12, *m/z* 878.5) containing DHA at both the sn1 and the sn2 positions of glycerol moiety was detected. PCs containing very long-chain PUFAs (PC 54:12, *m/z* 1018.8; PC 56:12, *m/z* 1046.7; PC 58:12, *m/z* 1074.9) were also observed in the crude lipid extract (Table 1). ESI MS analyses of the crude lipid extract also revealed the presence of phosphatidylethanolamine, phosphatidylserine, and phosphatidylinositol (**Table 2**, supplementary Figs. II–IV).

Identification of PCs along with their fatty acid composition was carried out by their MS/MS spectra obtained by LC-ESI MS negative ion mode. Negative ion mode MS/MS analysis provided the characteristic $[MX\text{-}CH_3X]^-$ ion from the precursor ion $[M+X]^-$, where X was a formate ion (HCO_2^-) (12). In the MS^3 stage, the product ion $[M\text{-}CH_3]^-$ was again used as a precursor ion and produced the fatty acyl ions and demethylated LPC ions (20, 21). The precursor ion at *m/z* 776.4 $[M+HCO_2]^-$ produced the product ion at *m/z* 716.5 $[M\text{-}CH_3]^-$; facile dissociation (CID) of this product ion gave the fatty acyl anions at *m/z* 255.3 (FA 16:0) and 253.4 (FA 16:1). Thus, the precursor ion at *m/z* 776.4 $[M+HCO_2]^-$ was identified as PC 32:1 (16:0/16:1) (supplementary Fig. V). The product ion also produced the demethylated LPC-related ions at *m/z* 480.5 and 462.2. Similarly, the other PC molecules were characterized as PC 32:0 (16:0/16:0), PC 34:1 (16:0/18:1), PC 34:2 (16:1/18:1), PC 36:1 (18:0/18:1), PC 36:4 (16:0/20:4), PC 38:6 (16:0/22:6), PC 40:6 (18:0/22:6), and PC 44:12 (22:6/22:6) (Table 1, supplementary Fig. V).

In the MS/MS spectrum of PC 34:2 (16:1/18:1, *m/z* 802.6), another coeluted isomer (16:0/18:2) was also

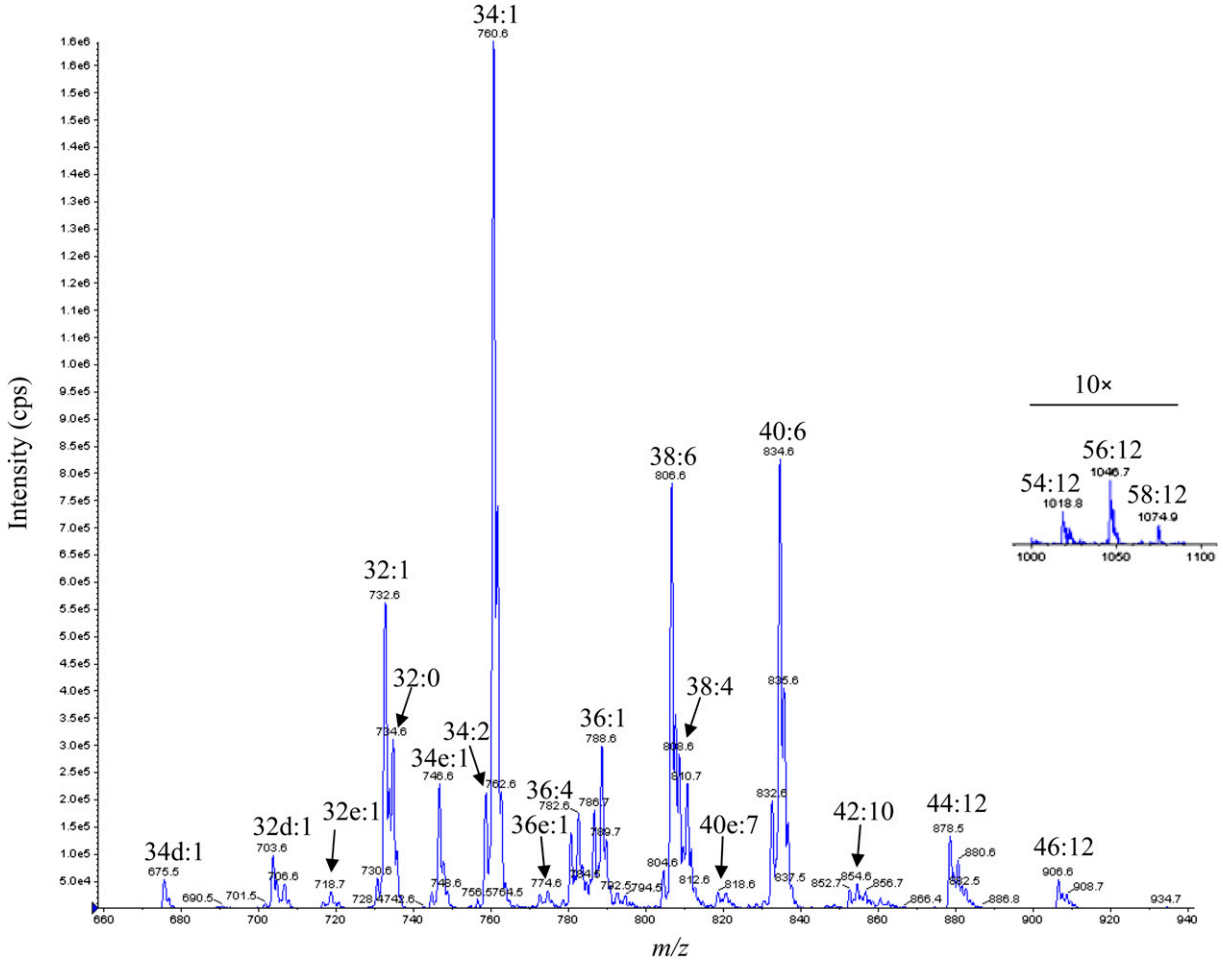

Fig. 2. Precursor ion scan ESI (+) mass spectrum of the salamander retina lipid extract by LC infusion.

observed. The product ion spectrum for *m/z* 922.6 (PC 44:12, 22:6/22:6) showed that the intensity of FA 22:6 anion is nearly the same in intensity correlating to one FA 22:6 (*m/z* 327.4) derived from PC 38:6 (*m/z* 850.6). This discrepancy was indeed supported by the MS/MS spectra taken from standard PCs (supplementary Fig. VI, VII). This might be due to a loss of only one of the FA 22:6 tails. In addition, a characteristic fragmentation pattern of PUFAs was observed in the MS/MS spectra, and all PCs containing PUFAs showed similar fragmentation behavior (supplementary Fig. V). For example, PC 44:12 (22:6/22:6, *m/z* 922.6) containing DHA gave the characteristic anions at *m/z* 327.3 (FA 22:6) and 283.4 ($[FA\ 22:6\text{-}CO_2]^-$) (24) along with other signals. A similar fragmentation pattern was also observed for PCs (*m/z* 826.6 and 854.6) containing FA 20:4 (product ions at *m/z* 283.4 and 259.4 [FA 20:4-CO_2]$^-$).

Distribution of phospholipids in the retina section

PCA is one of the multivariate analyses and categorizes a number of correlated variables into several principal components that are not correlated with each other. By applying PCA and displaying each component's "score" in a score-plot, one can distinguish particular regions in it and know the constituent ions (*m/z*) (4).

PCA of acquired MALDI IMS data provided several principal components with their contributed spectra. Among them, two significant principal components were selected. Their contributed spectra and distribution maps for six major phospholipids are shown in **Fig. 3**. All major lipids that were detected by MALDI MS were also observed in the crude lipid extract by ESI MS. Either PCA or manually picking up *m/z* values showed similar lipid distribution patterns in the retina section. As shown in Fig. 3, lipid ions at *m/z* 770.5 (PC 32:1), 772.5 (PC 32:0), and 798.5 (PC 34:1) were distributed mainly in the OPL and IPL layers of the retina. The other molecular ions at *m/z* 820.5 (PC 36:4), 844.5 (PC 38:6), and 872.5 (PC 40:6) were distributed mainly in the OS, IS, and RPE layers. However, distribution of PC 36:4, PC 38:6, and PC 40:6 in the three retinal layers might be due to intermingling of these layers.

Endogenous alkali metals form a significant amount of adducts with lipids and contribute in the MALDI mass spectrum. Thus, the effect of endogenous alkali metals forming adducts with lipids in three retinal layers was examined. A very similar contribution of Na^+ and K^+ forming adducts with phospholipids was found in each retinal layer. For example, in the IPL layer, PC 34:1 molcule forming ions at *m/z* 798.5 $[M+K]^+$, 782.5 $[M+Na]^+$, and 760.5 $[M+H]^+$ contributed about 64, 29, and 7% respectively, in

TABLE 1. Choline containing phospholipid species in the salamander retina detected by MS

		ESI		AP MALDI		
Lipid	FA/FA	$[M+H]^+$	$[M+HCO_2]^-$	$[M+K]^+$	$[M+Na]^+$	$[M+H]^+$
34d:1	d18:1/16:0	675.5	719.8			
32d:1	d18:1/14:0	703.6	747.8			
32e:1	alkyl16:0/16:1	718.6	762.8			
32:1	16:0/16:1	732.6	776.8	770.5	754.5	–[d]
32:0	16:0/16:0	734.6	778.8	772.5	756.5	–[d]
34e:1	alkyl16:0/18:1	746.6	790.8			
34:2	16:1/18:1	758.6	802.8	–[c]	–[c]	
34:1	16:0/18:1	760.6	804.9	798.5	782.5	760.5
36e:1	alkyl18:0/18:1	774.6	818.9			
36:4	16:0/20:4	782.6	826.8	820.5	804.5	782.6
36:1	18:0/18:1	788.6	832.9			
38:6	16:0/22:6	806.6	850.8	844.5	828.5	–[d]
38:4	18:0/20:4	808.6	852.8			
40e:7	alkyl18:1/22:6	818.6	862.8			
40:6	18:0/22:6	834.6	878.9	872.5	856.5	–[d]
42:10	20:4/22:6[a]	854.6	898.8			
44:12	22:6/22:6	878.5	922.8			
46:12	24:6/22:6[a]	906.6	950.8			
54:12	32:6/22:6[a]	1018.8	–[b]			
56:12	34:6/22:6[a]	1046.7				
58:12	36:6/22:6[a]	1074.9				

[a]Tentative composition of fatty acid.
[b]Not measured.
[c]Not observed due to low abundance.
[d]$[M+H]^+$ ions contributed only $0 \leq 10\%$ in the spectrum.

the mass spectrum. This lipid also showed similar alkali metal adducts formation in the OPL and INL layers. The other lipid also formed alkali metal adducts throughout the retinal layers in a similar fashion (**Table 3**). It is worth mentioning that the adduct formation affinity of metal ions with lipids containing PUFAs was somewhat different from lipids containing saturated or monounsaturated fatty acids (supplementary Table I). These results indicated that we observed lipid distribution throughout the retinal tissue rather than alkali metals distribution.

Mosaic distribution of phospholipids in the OS and IS regions

It was difficult to differentiate the distribution of lipids in the IS, OS, and RPE layers because of their intercrossing. To detect specific lipid composition on the IS and OS layers of the salamander retina, MALDI raster scanning was focused on the IS and OS layers (**Fig. 4A**, area in circles). Three major phospholipids containing PUFAs at *m/z* 820.5 (PC 36:4), 844.5 (PC 38:6), and 872.5 (PC 40:6) were detected in the OS and IS regions (Fig. 4). These lipids were highly populated over 50% of the total pixels (30 × 6) in the given scanned area and showed their discrete distribution with a variable intensity over the scanned area. Among the three PC species, PC (38:6) and PC (40:6) were the most abundant lipids (Fig. 4B). Both lipids were localized on the basal part of photoreceptor cells whereas the other PC 36:4 was concentrated on the apical part. These lipids' localization is consistent with the whole retina imaging map, as shown in Fig. 3. At the pixel 45, the signal intensity of PC 38:6 was relatively faint compared with PC 36:4 and PC 40:6 signals, indicating its low abundance at this position (Fig. 4B, arrow). The relative intensity of each molecular ion (*m/z*) indicated its relative abundance in the particular cell or cell part at each pixel (Fig. 4C). Each circle (laser spot) could be considered to cover a single cell or a part of a single cell, and a relative lipid composition in a particular spot might indicate its lipids profile. Empty spots/circles could be a result of low lipid content, poor matrix distribution,

TABLE 2. Other major phospholipids species in the salamander retina lipid extract detected by ESI (+) MS

Lipid	FA/FA[a]	$[M+H]^+$	Lipid	FA/FA[a]	$[M+H]^+$
	Phosphatidylethanolamine			Phosphatidylserine	
34:1	16:0/18:1	718.5	40:6	20:3/20:3	836.6
36:2	18:1/18:1	744.5	44:12	22:6/22:6	880.4
38:6	18:1/20:5	764.5	44:11	22:6/22:5	882.5
38:5	18:0/20:5	766.6	46:12	22:6/24:6	908.6
38:4	18:0/20:4	768.6	46:11	22:6/24:5	910.5
40:6	20:3/20:3	792.6		Phosphatidylinositol	
42:10	22:6/20:4	812.5	36:4	16:0/20:4	876.7
44:12	22:6/22:6	836.6	38:4	18:0/20:4	904.7
44:11	22:6/22:5	838.6	38:5	18:1/20:4	902.8
46:12	22:6/24:6	864.6	40:6	20:3/20:3	928.6

[a]Tentative composition of fatty acid.

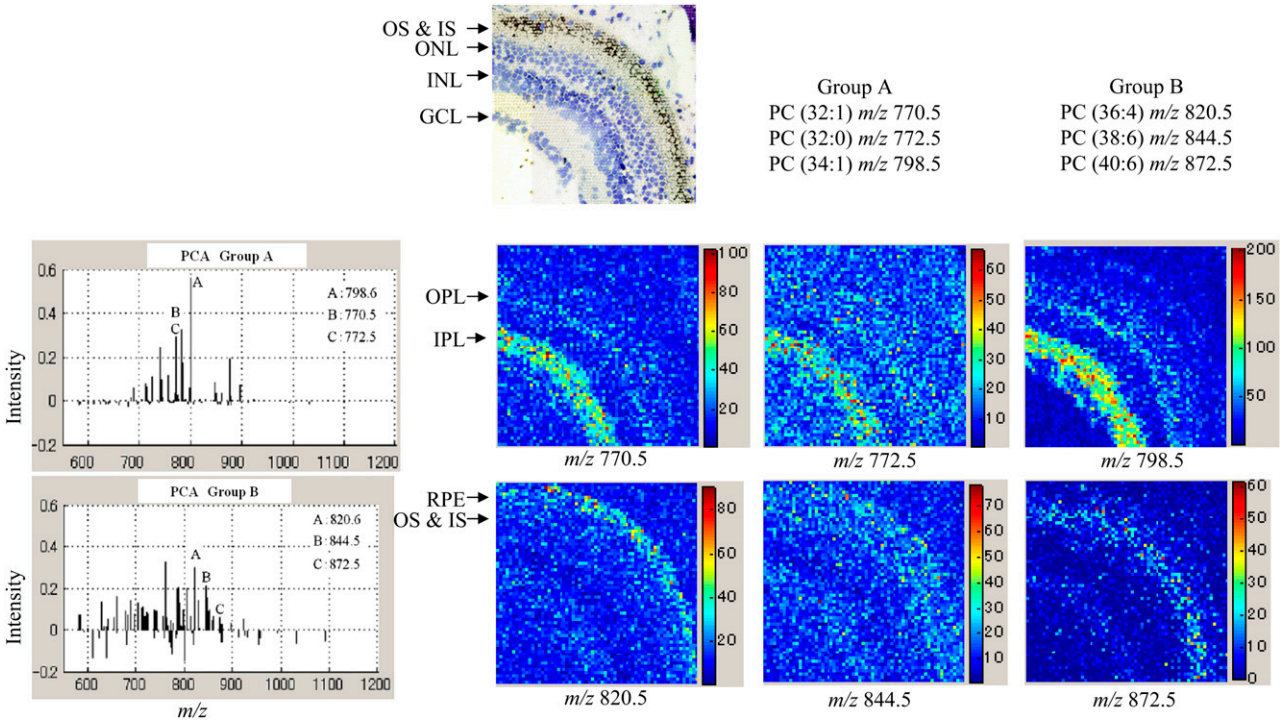

Fig. 3. Image reconstruction of phospholipids distribution in the salamander retina section. PC 32:0, PC 32:1, and PC 34:1 are distributed in the OPL and IPL layers; PC 36:4, PC 38:6, and PC 40:6 are distributed in the IS, OS, and RPE layers. Inset is an optical image of salamander retina section. Raw intensity was used.

absence of matrix, or laser irradiation on an intercellular space.

DISCUSSION

Phospholipids content and composition of the salamander retina lipid extract showed high similarity with that of the rat retina lipid extract (12). Detection of lipids containing long- and very long-chain PUFAs that associated with rhodopsin was consistent with bovine retina lipids (25). Major lipid species along with their fatty acid compositions were identified on the basis of their *m/z*, MS/MS data, and database search (23) (Tables 1, 2). Among them, six major lipids were detected and localized in the AP MALDI IMS measurement. PCA of MALDI IMS data found the same phospholipids peaks as detected in the crude lipid extract by ESI MS. Thus, PCA is a useful tool to find significant molecular peaks from principal components without previous knowledge of molecules.

Lipids containing PUFA acyl moieties were observed mostly in both the OS and the IS layers, which is consistent with previous findings (13). The OS layer harboring rhodopsin, where phototransduction process occurs, is composed of lipids containing mainly PUFAs (5–7). The phototransduction process involving conformational changes of rhodopsin is largely facilitated by a sufficiently flexible lipid bilayer, and the lipid bilayer fluidity is mostly dependent on the composition of phospholipids' fatty acyl groups. Phospholipids composing PUFAs like DHA, with low gel-to-fluid properties (26), provide sufficient fluidity of the lipid bilayer and play significant roles in the phototransduction process (8). Thus, the specific presence of lipids containing PUFAs in the OS and IS layers indicates that these lipids form the flexible lipid bilayers and their different compositions might indicate their cell and cell part specificity in the OS and IS layers. However, identification of particular cell types through their lipid profiles is beyond the scope of this present work. Further research is necessary to clarify the cell specific lipid profile.

The large cells of the salamander allowed us to identify and localize lipids in the retinal layers at cellular size resolution. By considering the tissue section thickness (5 μm), which is smaller than the salamander retinal cell (14 μm), a single cell level analysis could be achieved, as shown in Fig. 4.

TABLE 3. Average contribution (%) of alkali metals forming adducts with phospholipids species in the salamander retina section observed in MALDI MS spectrum

	PC 34:1			PC 32:1		
Layer	$[M+K]^+$	$[M+Na]^+$	$[M+H]^+$	$[M+K]^+$	$[M+Na]^+$	$[M+H]^+$
IPL	64	29	7	68	32	0
OPL	68	25	7	71	29	0
INL	76	24	0			

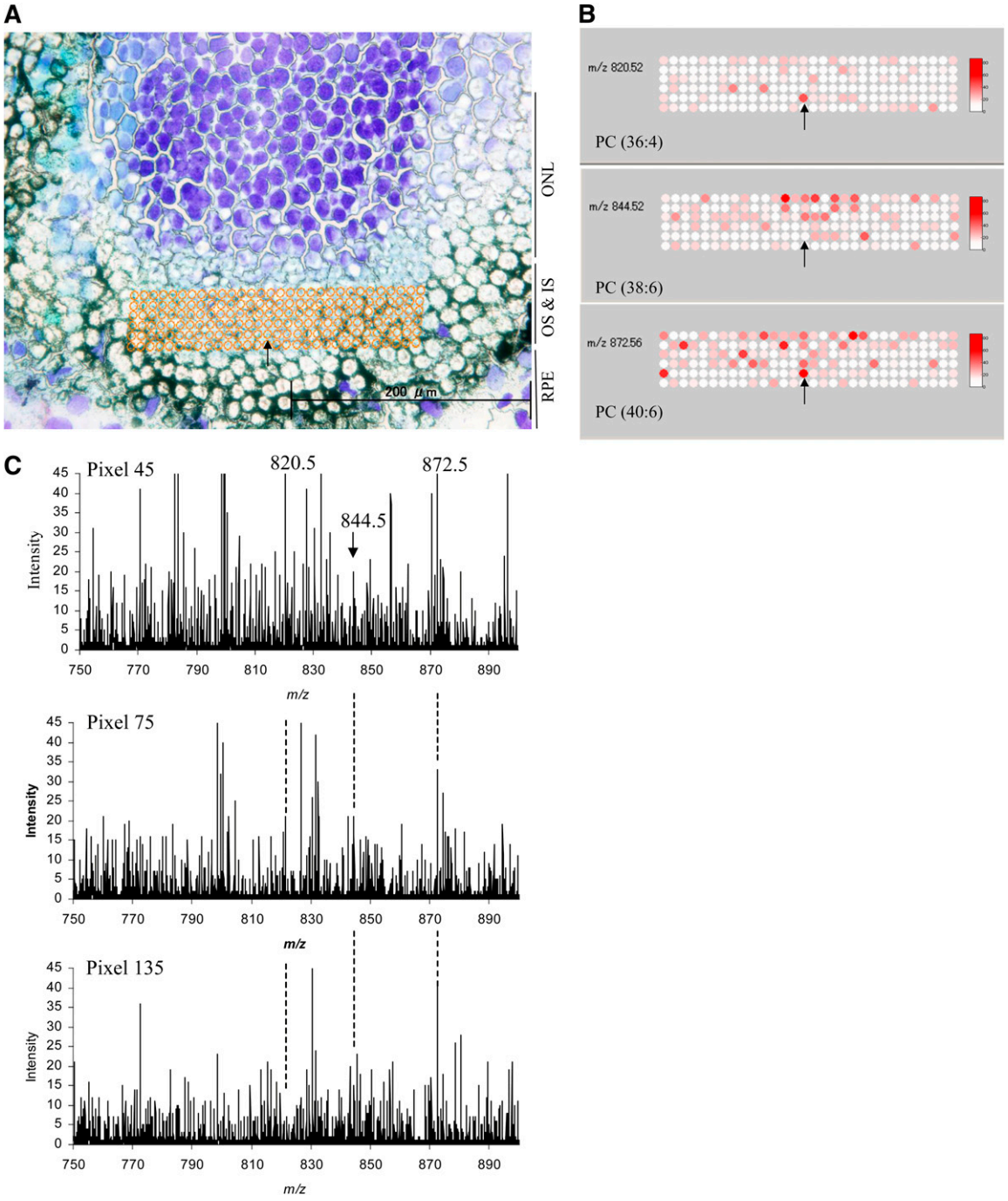

Fig. 4. A: Focused raster scanning area is shown as circles in the OS and IS layers. B: Mosaic distribution of phospholipids in the OS and IS layers is shown, the area corresponds to the circles as shown in (A). PC 36:4, PC 38:6, and PC 40:6 are unevenly distributed at the pixel 45 (arrow). C: Single spot MALDI MS spectra of lipids are shown. Each MS spectrum corresponds to a particular pixel as shown in (A) and (B). Pixel 45 (arrow), pixel 75 (2nd circle above the arrow), and pixel 135 (4th circle above the arrow) show the corresponding lipid ions with different intensities. Detail pixel number is given in supplementary Fig. XIII.

The highly focused laser beam gave imaging capacity within a small area (7 μm). However, the major limitations of the small laser spot are significant decrease of ion population of mass signals and an increase in experimental time. With a significant reduction of ion population from a 7 μm spot, MS/MS data analysis is more difficult. Identification of low abundant lipids was also impractical due to very low intensity of mass signals.

ESI MS data of the salamander retina crude lipid extract are complementary to MALDI MS data obtained directly from the salamander retina section. It is useful to have ESI and MALDI MS methods in combination to get a relatively complete lipid profile of tissue/cell, particularly where MALDI MS could not provide useful MS/MS information. The ESI MS analysis showed a much richer lipid profile of the salamander retina than the MDLDI MS. In this study,

we focused only on the major PC analysis by MALDI MS. Analysis of other classes of lipids (e.g., PE, PS, and PI) along with low abundant lipids deserves further research. It is suggested that these lipids undergo cleavage during ionization from matrix (DHB) (27). Thus, their analysis could be achieved using other matrix and negative ion mode MALDI.

In conclusion, identification and molecular profiling of a particular cell or cell types using MALDI IMS would be an interesting future research area, and the salamander, having large cells, could be an ideal model animal for IMS analysis and profiling of biomolecules in a given tissue and/or cell.

The authors thank Dr. Makoto Araki, Okinawa Institute of Science and Technology, for his cooperation on the collection of the salamander retina samples.

REFERENCES

1. Han, X., and R. W. Gross. 2005. Shotgun lipidomics: electrospray ionization mass spectrometric analysis and quantitation of cellular lipidomes directly from crude extracts of biological samples. *Mass Spectrom. Rev.* **24:** 367–412.
2. Han, X., and R. W. Gross. 2003. Global analyses of cellular lipidomes directly from crude extracts of biological samples by ESI mass spectrometry: a bridge to lipidomics. *J. Lipid Res.* **44:** 1071–1079.
3. Schwudke, D., J. Oegema, L. Burton, E. Entchev, J. T. Hannich, C. S. Ejsing, T. Kurzchalia, and A. Shevchenko. 2006. Lipid profiling by multiple precursor and neutral loss scanning driven by the data-dependent acquisition. *Anal. Chem.* **78:** 585–595.
4. Trim, P. J., S. J. Atkinson, A. P. Princivalle, P. S. Marshall, A. West, and M. R. Clench. 2008. Matrix-assisted laser desorption/ionisation mass spectrometry imaging of lipids in rat brain tissue with integrated unsupervised and supervised multivariant statistical analysis. *Rapid Commun. Mass Spectrom.* **22:** 1503–1509.
5. Martin, R. E., S. J. Fliesler, R. S. Brush, M. J. Richards, S. A. Hopkins, and R. E. Anderson. 2005. Lipid differences in rod outer segment membranes of rats with P23H and S334ter opsin mutations. *Mol. Vis.* **11:** 338–346.
6. Organisciak, D. T., R. M. Darrow, Y. L. Jiang, and J. C. Blanks. 1996. Retinal light damage in rats with altered levels of rod outer segment docosahexaenoate. *Invest. Ophthalmol. Vis. Sci.* **37:** 2243–2257.
7. Rotstein, N. P., M. I. Aveldaflo, F. J. Barrantes, and L. E. Politi. 1996. Docosahexaenoic acid is required for the survival of rat retinal photoreceptors in vitro. *J. Neurochem.* **66:** 1851–1859.
8. Botelho, A. V., N. J. Gibson, R. L. Thurmond, Y. Wang, and M. F. Brown. 2002. Conformational energetics of rhodopsin modulated by nonlamellar-forming lipids. *Biochemistry.* **41:** 6354–6368.
9. Suzuki, M., M. Kamei, H. Itabe, K. Yoneda, H. Bando, N. Kume, and Y. Tano. 2007. Oxidized phospholipids in the macula increase with age and in eyes with age-related macular degeneration. *Mol. Vis.* **13:** 772–778.
10. Pan, H. Z., H. Zhang, D. Chang, H. Li, and H. Sui. 2008. The change of oxidative stress products in diabetes mellitus and diabetic retinopathy. *Br. J. Ophthalmol.* **92:** 548–551.
11. Busik, J. V., G. E. Reid, and T. A. Lydic. 2009. Global analysis of retina lipids by complementary precursor ion and neutral loss mode tandem mass spectrometry. *Methods Mol. Biol.* **579:** 33–70.
12. Lydic, T. A., J. V. Busik, W. J. Esselman, and G. E. Reid. 2009. Complementary precursor ion and neutral loss scan mode tandem mass spectrometry for the analysis of glycerophosphatidylethanolamine lipids from whole rat retina. *Anal. Bioanal. Chem.* **394:** 267–275.
13. Hayasaka, T., N. Goto-Inoue, Y. Sugiura, N. Zaima, H. Nakanishi, K. Ohishi, S. Nakanishi, T. Naito, R. Taguchi, and M. Setou. 2008. Matrix-assisted laser desorption/ionization quadrupole ion trap time-of-flight (MALDI-QIT-TOF)-based imaging mass spectrometry reveals a layered distribution of phospholipid molecular species in the mouse retina. *Rapid Commun. Mass Spectrom.* **22:** 3415–3426.
14. Hayasaka, T., N. Goto-Inoue, N. Zaima, K. Shrivas, Y. Kashiwagi, M. Yamamoto, M. Nakamoto, and M. Setou. 2010. Imaging mass spectrometry with silver nanoparticles reveals the distribution of fatty acids in mouse retinal sections. *J. Am. Soc. Mass Spectrom.* **21:** 1446–1454.
15. Li, Y., B. Shrestha, and A. Vertes. 2008. Atmospheric pressure infrared MALDI imaging mass spectrometry for plant metabolomics. *Anal. Chem.* **80:** 407–420.
16. Nemes, P., A. S. Woods, and A. Vertes. 2010. Simultaneous imaging of small metabolites and lipids in rat brain tissues at atmospheric pressure by laser ablation electrospray ionization mass spectrometry. *Anal. Chem.* **82:** 982–988.
17. Mikawa, S., M. Suzuki, C. Fujimoto, and K. Sato. 2009. Imaging of phosphatidylcholines in the adult rat brain using MALDI-TOF MS. *Neurosci. Lett.* **451:** 45–49.
18. Hankin, J. A., R. M. Barkley, and R. C. Murphy. 2007. Sublimation as a method of matrix application for mass spectrometric imaging. *J. Am. Soc. Mass Spectrom.* **18:** 1646–1652.
19. Bligh, E. G., and W. J. Dyer. 1959. A rapid method of total lipid extraction and purification. *Can. J. Biochem. Physiol.* **37:** 911–917.
20. Taguchi, R., T. Houjou, H. Nakanishi, T. Yamazaki, M. Ishida, M. Imagawa, and T. Shimizu. 2005. Focused lipidomics by tandem mass spectrometry. *J. Chromatogr. B Analyt. Technol. Biomed. Life Sci.* **823:** 26–36.
21. Houjou, T., K. Yamatani, H. Nakanishi, M. Imagawa, T. Shimizu, and R. Taguchi. 2004. Rapid and selective identification of molecular species in phosphatidylcholine and sphingomyelin by conditional neutral loss scanning and MS3. *Rapid Commun. Mass Spectrom.* **18:** 3123–3130.
22. Harada, T., A. Yuba-Kubo, Y. Sugiura, N. Zaima, T. Hayasaka, N. Goto-Inoue, M. Wakui, M. Suematsu, K. Takeshita, K. Ogawa, et al. 2009. Visualization of volatile substances in different organelles with an atmospheric-pressure mass microscope. *Anal. Chem.* **81:** 9153–9157.
23. R. Taguchi Group, Tokyo University. Lipid search tool. Accessed May 2010 at http://lipidsearch.jp/manual_search/.
24. Ejsing, C. S., E. Duchoslav, J. Sampaio, K. Simons, R. Bonner, C. Thiele, K. Ekroos, and A. Shevchenko. 2006. Automated identification and quantification of glycerophospholipid molecular species by multiple precursor ion scanning. *Anal. Chem.* **78:** 6202–6214.
25. Aveldano, M. I. 1988. Phospholipid species containing long and very long polyenoic fatty acids remain with rhodopsin after hexane extraction of photoreceptor membranes. *Biochemistry.* **27:** 1229–1239.
26. Bakht, O., P. Pathak, and E. London. 2007. Effect of the structure of lipids favoring disordered domain formation on the stability of cholesterol-containing ordered domains (lipid rafts): identification of multiple raft-stabilization mechanisms. *Biophys. J.* **93:** 4307–4318.
27. Murphy, R. C., J. A. Hankin, and R. M. Barkley. 2009. Imaging of lipid species by MALDI mass spectrometry. *J. Lipid Res.* **50:** S317–S322.